Gulf of Alaska Coastal Water Transport Pathways and Implications for Ecosystem Response

ÉLISE BEAUDIN,[a,b] EMANUELE DI LORENZO,[b] MARA A. FREILICH,[b,c] AND ARTHUR J. MILLER[d]

[a] *Ocean Networks Canada, University of Victoria, Victoria, British Columbia, Canada*
[b] *Department of Earth, Environmental and Planetary Sciences, Brown University, Providence, Rhode Island*
[c] *Division of Applied Mathematics, Brown University, Providence, Rhode Island*
[d] *Scripps Institution of Oceanography, University of California, San Diego, San Diego, California*

(Manuscript received 18 March 2026, in final form 15 August 2026, accepted 2 September 2026)

ABSTRACT: The Alaska subpolar gyre is a high-nutrient, low-chlorophyll system in which offshore productivity depends on exchange with iron- and macronutrient-rich coastal waters. Mesoscale eddies are the primary mechanism for export of nutrient-rich coastal waters offshore, and their formation is strongly linked to large-scale atmospheric forcing associated with the Aleutian low (AL), which seasonally modulates regional wind stress, circulation, and eddy generation. Recent marine heat waves, including the 2013–14 Blob, the 2015/16 El Niño, and the 2019 Alaska heat wave, were associated with distinct climate anomalies that altered atmospheric circulation and modulated the AL, raising questions about how coastal export responds to prolonged climate extremes. Here, we examine variability in the Gulf of Alaska coastal transport pathways over 1993–2025, using Lagrangian particle tracking in a high-resolution ocean reanalysis product. We identify three dominant pathways: transport along the mean gyre circulation, offshore export via mesoscale eddies, and coastal retention. Variability in these pathways is primarily linked to atmospheric sea level pressure, local wind stress and wind stress curl, and eddy kinetic energy. Despite weakened circulation and reduced eddy formation during the prolonged marine heat wave conditions between 2013 and 2019, offshore export through the eddy pathway persisted and even periodically intensified during El Niño events. In contrast, transport along the mean gyre circulation declined significantly. These findings suggest that the reorganization of ocean transport pathways can act as a dynamic resilience mechanism for ecosystem response during such extreme conditions.

SIGNIFICANCE STATEMENT: This study examines how persistent high pressure anomalies associated with northeast Pacific marine heat waves and weakened Aleutian low affected the transport of macronutrient-rich (e.g., iron) coastal waters into the macronutrient-limited Alaska subpolar gyre. Our results show that transport of coastal waters into the basin interior is linked to large-scale wind forcing, El Niño variability, and wind stress curl. Because travel times from the shelf break to the basin interior can span several years, these export pathways may provide a basis for seasonal-to-interannual predictability of ecosystem responses during future extreme events. Future work should examine how circulation changes under different climate regimes influence ecosystem productivity and biogeochemical cycling.

KEYWORDS: North Pacific Ocean; Lagrangian circulation/transport; Extreme events; El Niño

1. Introduction

The Gulf of Alaska (GOA) is a highly productive region where mesoscale eddies play a key role in exporting nutrient-rich coastal waters into the nutrient-depleted basin interior (Combes and Di Lorenzo 2007). These eddies, primarily anticyclonic, originate near the coast (Haida Gwaii and Sitka regions) and transport iron-rich water offshore, supporting biological productivity (Boyd et al. 1995; Whitney and Robert 2002; Crawford 2005; Ladd 2007; Cullen et al. 2009; Ito et al. 2026). In the recent decade (2013–24), the GOA has experienced a series of record-breaking marine heat waves (MHWs) and circulation changes, driven by persistent high sea level pressure anomalies (SLPa). These events include the 2013–14 Blob (Bond et al. 2015), the 2015/16 El Niño (Di Lorenzo and Mantua 2016; Hayes et al. 2025), and the 2019 Alaska heat wave (Amaya et al. 2020). Specifically, the persistent high SLPa associated with the weakened Aleutian low (AL) during the 2013–14 MHW reduced wintertime ocean heat loss and upper-ocean cooling, which increased surface warming. The thermodynamic consequences (e.g., increased surface heat content, stratification, reduced mixing) and their impacts on marine ecology (e.g., fisheries collapse, ecological shifts, mass mortality) have been well documented (Suryan et al. 2021;Weitzman et al. 2021; McKinstry et al. 2022; Batten et al. 2022;Wyatt et al. 2022; Almeida et al. 2024; Hauri et al. 2024). However, less is known about the associated changes in dynamics, including eddy-scale and gyre-scale transport and the redistribution of coastal water across the basin.

Mesoscale eddies are typically generated in spring, following strong downwelling-favorable winter winds that elevate coastal sea surface height (SSH). This creates a strong cross-shore gradient, which, in turn, intensifies the gyre circulation and the meandering

Denotes content that is immediately available upon publication as open access.

Supplemental information related to this paper is available at the Journals Online website: https://doi.org/10.1175/JPO-D-26-0059.s1.

Corresponding author: Élise Beaudin, ebeaudin@oceannetworks.ca

DOI: 10.1175/JPO-D-26-0059.1

© 2026 American Meteorological Society. This published article is licensed under the terms of the default AMS reuse license. For information regarding reuse of this content and general copyright information, consult the AMS Copyright Policy (www.ametsoc.org/PUBSReuseLicenses).

Unauthenticated | Downloaded 11/19/26 07:19 PM UTC

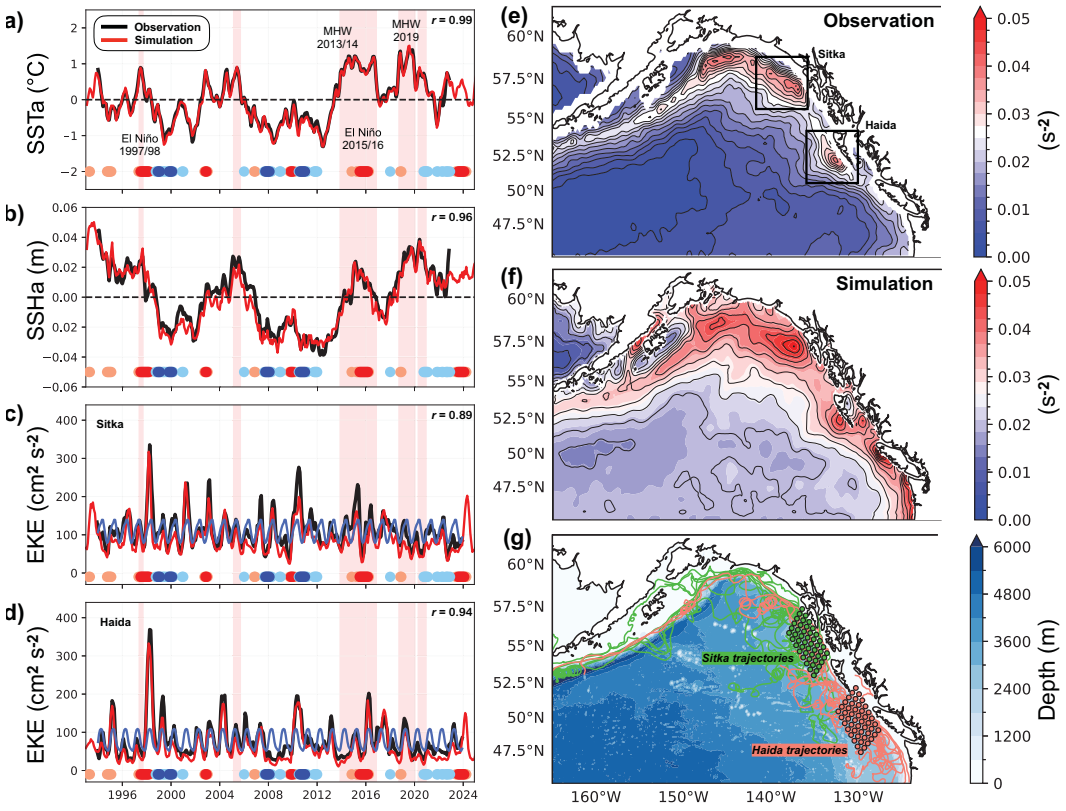


FIG. 1. Comparison between reanalysis product and observations of GOA (a) SSTa, (b) SSHa, and EKE at (c) Sitka and (d) Haida regions, averaged over areas in (e), and observed climatologies (blue). The GOA region is defined as 40°–70°N and 170°–120°W, excluding the Bering Sea. Strong and weak El Niño events are shown in dark and light red dots at the panel bottom, respectively, while strong and weak La Niña events are shown in dark and light blue dots, respectively. Shaded red areas represent periods where SSTa was larger than one standard deviation for at least five consecutive months. (e) The observed $|\partial(\zeta/f)/\partial t|$ is shown; (f) as in (e), but for the reanalysis product comparison. (g) A subset of trajectories along with the release sites are shown, pink for Haida and green for Sitka, with bathymetry contours.

Alaska Current (Stabeno et al. 2004; Combes et al. 2009). As this current strengthens, it eventually becomes baroclinically unstable and generates mesoscale anticyclonic eddies (Ladd et al. 2009). These eddies contain a relatively warm and fresh core around 100-m depth and propagate away from the coastline up to 1000 km westward for up to several years (Tabata 1982; Crawford et al. 2002; Okkonen et al. 2003; Ladd 2007; Rovegno et al. 2009). This eddy generation mechanism has been linked to variability in the large-scale atmospheric conditions over seasonal and interannual time scales, including variability in the AL (Combes and Di Lorenzo 2007; Ueno et al. 2009) as well as local processes such as coastal wind stress variability (Combes et al. 2009). The recent weakening of the AL was found to be linked to a suppression of the overall mesoscale eddy field (Rallu De Malibran et al. 2024), suggesting a potential link to ecosystem dynamics through modified transport pathways. However, the mechanisms underlying the link between sea level pressure (SLP) changes and eddy kinetic energy (EKE) changes and the role of these changes in offshore nutrient supply and their subsequent impact on ecosystem dynamics remain open questions.

In this study, we test the hypothesis that periods of extreme atmospheric forcing in the GOA led to changes in eddy-scale dynamics, altering transport pathways and redistribution of coastal water masses. We address this by using Lagrangian particle trajectories released in an ocean reanalysis product from two coastal eddy formation regions: Haida Gwaii and Sitka (Fig. 1e) and trace export pathway variability under anomalous large-scale atmospheric forcings. Our goal is to 1) characterize the dominant export pathways, 2) assess their seasonality and interannual variability, and 3) identify and quantify the contribution of atmospheric and oceanic forcings on transport regimes.

This paper is organized as follows. In section 2, we describe the data and methods used in this analysis. In section 3a, we validate the ocean reanalysis product's ability to reproduce the observed changes in sea surface temperature (SST), SSH, and EKE. In section 3b, we group the trajectories into dominant transport pathways and evaluate their variability. Last, in section 3c, we develop a linear regression model to evaluate how external forcings control the likelihood of each pathway. Here, we show that the transport pathways of coastal waters in the Gulf of Alaska are controlled by various

Unauthenticated | Downloaded 11/19/26 07:19 PM UTC

forcings, with cross-shelf exchange persisting through marine heat waves.

2. Data and methods

a. Datasets

1) Observational datasets

The eddy variability in the GOA is examined through satellite-derived EKE from SSH and surface geostrophic current data from the Global Ocean Gridded L4 Sea Surface Heights and Derived Variables Reprocessed by Copernicus Climate Service (https://doi.org/10.48670/moi-00145). The data are at monthly temporal resolution and with a horizontal average resolution of 1/4°, from 1993 to 2024. SSH anomalies (SSHa) were computed by removing monthly climatology from the full SSH time series. The climatology was calculated at each grid point over the period 1993–2024, after detrending the SSH to remove the long-term steric-height effect.

Additionally, for model validation, monthly averages of SST between 1993 and 2025 are obtained from the Multi Observation Global Ocean ARMOR3D L4 analysis and multi-year reprocessing, by Copernicus Climate Service (https://doi.org/10.48670/moi-00052), with a horizontal resolution of 1/8°. Anomalies are computed by removing monthly averages over the full time period.

The atmospheric forcings over the northeast Pacific are examined using monthly averages of SLP and turbulent surface stresses from the ERA5 reanalysis product (https://doi.org/10.24381/cds.f17050d7), gridded at a 1/4° horizontal resolution, available from 1940 to the present. In this study, we use the 1993–2024 period, to match the ocean reanalysis and satellite era.

2) Ocean velocity product

To simulate Lagrangian transport pathways, we used daily flow fields from the Global Ocean Reanalysis and Simulations (GLORYS) 12V1 ocean reanalysis product (Jean-Michel et al. 2021, https://doi.org/10.48670/moi-00021). This reanalysis product has a horizontal resolution of 1/12° and 50 vertical levels, allowing the representation of mesoscale eddies with characteristic spatial scales of $\mathcal{O}(100)$ km, as well as mesoscale coastal circulation dynamics (such as regional cross-shelf exchange), while small islands and narrow inlet dynamics remain unresolved at this resolution. GLORYS12V1 uses the ECMWF ERA-Interim and ERA5 reanalysis products for surface atmospheric forcing and assimilates along-track satellite altimetry, SST, and sea ice concentration from satellite observations as well as in situ profiles of temperature and salinity. The assimilation cycle is 7 days, including the incremental analysis update (IAU) scheme that redistributes the analysis correction over the assimilation window, smoothing out discontinuities in the velocity field (Jean-Michel et al. 2021). The horizontal resolution accounts for roughly 6 km in the GOA, which is good enough to resolve the complex coastal dynamics and the mesoscale eddies.

b. Upwelling/downwelling conditions

An index of upwelling- and downwelling-favorable conditions is derived following Rallu De Malibran et al. (2024). Downwelling conditions in the GOA are associated with a sustained strong AL and high EKE, while upwelling conditions are associated with sustained weak AL often leading to MHWs. The index is obtained by identifying the SLPa pattern associated with variability in the Alaska Stream Current through spatial correlation analysis and then projecting this pattern onto the time-dependent SLPa field (Fig. S3 in the online supplemental material). Positive (negative) values of the index correspond to downwelling- (upwelling-) favorable atmospheric conditions. Periods of persistent upwelling or downwelling are defined as intervals during which the index retains the same sign for at least five consecutive months; otherwise, the sign reversal is not considered a regime transition.

c. Lagrangian model setup

We investigate the transport of coastal water masses in the Gulf of Alaska using a Lagrangian particle tracking experiment. Each day, from 1993 to 2025, we release 48 particles in each of the Haida and Sitka coastal regions (Fig. 1g) and are advected forward in time using a fourth-order Runge–Kutta scheme on daily time steps. The advection is done on a 2D velocity field from the GLORYS12V1 ocean reanalysis product. The particles are treated as passive tracers without assigned size, buoyancy, or inertia and therefore follow the resolved flow field directly. Sensitivity tests (Fig. S2) show consistent basin-scale trajectory patterns across depths from the surface to 100 m, with dominant transport pathways following the Alaska Gyre circulation and offshore export through mesoscale eddies, filaments, and entrainment. Surface velocities are more strongly influenced by direct wind forcing. Since our objective is to investigate geostrophically driven transport pathways, particles are seeded at 50-m depth, representative of the typical eddy core depth in this region (Crawford et al. 2002).

The seeding regions were selected to overlap with areas of permanent meanders and mesoscale Haida and Sitka eddy formation regions. This is where coastal waters become entrained into the Alaska Current and mesoscale circulation. These regions are also consistent with the observed offshore extension of elevated chlorophyll concentrations and modeled subsurface iron-rich coastal waters (Combes et al. 2009; Ito et al. 2026).

Lagrangian trajectories are computed using horizontal velocities only. This is a reasonable assumption for mesoscale lateral transport, as vertical velocities associated with mesoscale eddies in the Gulf of Alaska are typically an order of magnitude smaller than the horizontal velocities.

A total of 566 400 particles are released and tracked over the study period. To prevent particles from crossing onto land due to numerical artifacts, we apply a cross-coastline velocity mask that removes onshore velocity components in the nearest grid cell to the coastline: Eastward u velocities west of the coastline are set to zero, westward u velocities east of it, northward v velocities south of it, and southward v velocities north of it. This procedure helps remove most of the onshore particle trajectories, although some remain but are insignificant. This method

Unauthenticated | Downloaded 11/19/26 07:19 PM UTC

TABLE 1. Classification of particles released from Haida Gwaii and Sitka based on transport types.

Release area	Name	Classification criteria	Physical mechanisms
Haida Gwaii	Gyre Circulation	Particles crossing 56°N after 60 days	Rapid advection within the Alaskan Stream
Haida Gwaii	Offshore Export	Particles south of 56°N after 60 days and west of 132°W	Cross-shelf exchange mediated by mesoscale Haida eddies, jet meanders, and offshore filaments
Haida Gwaii	Coastal Retention	Particles south of 56°N and east of 132°W	Local retention near release site; slow or recirculating transport
Sitka	Gyre Circulation	Particles reaching west of 144°W and north of 58°N within 90 days	Rapid advection within the Alaskan Stream
Sitka	Offshore Export	Particles not crossing west of 144°W or north of 58°N within 60 days, but north of 53°N	Cross-shelf exchange mediated by mesoscale Sitka eddies, jet meanders, and offshore filaments
Sitka	Southward Coastal Retention	Particles crossing south of 53°N within 30 days without moving west of 144°W	Unusual southward pathway in otherwise northwestward circulation

can cause another numerical artifact where some particles can get "stuck," meaning that they recirculate indefinitely especially near the coastline and islands. Particles that remain within a 5-km radius for three consecutive days are excluded from subsequent integration steps. Similarly, particles that exit the domain are also excluded.

d. Pathway definitions

For each release site, we classify particle trajectories into three distinct transport pathways based on their spatial evolution following release, using latitude and longitude thresholds defined in Table 1. These specific temporal windows and criteria were selected to align with empirical transit times for particles to migrate from their coastal release areas into the basin interior (discussed further in section 4). These pathways are not defined according to the geometry of the domain but instead to reflect established circulation patterns and mesoscale variability in the region: alongshore advection, offshore export, and coastal retention.

e. Linear regression model

We use a linear regression model to evaluate the relative influence of external forcings on the occurrence of specific particle trajectory pathways. The model assumes a linear relationship between the predictors and the response variable:

$$\mathbf{y} = \mathbf{X}\boldsymbol{\beta} + \boldsymbol{\varepsilon}, \tag{1}$$

and the coefficients are obtained by minimizing the sum of squared residuals:

$$\boldsymbol{\beta} = (\mathbf{X}^{\mathrm{T}}\mathbf{X})^{-1}\mathbf{X}^{\mathrm{T}}\mathbf{y}, \tag{2}$$

where $\mathbf{y}$ is the observed fractions of trajectories assigned to each pathway cluster (Table 1), $\mathbf{X}$ is the matrix of predictors, $\boldsymbol{\varepsilon}$ is the error term, and $\boldsymbol{\beta}$ contains the regression coefficients. All predictors are standardized prior to regression, which allows for a direct comparison of their relative contributions. For this study, the predictors include GOA SLPa, local meridional wind stress anomalies (τ_{y_ano}), wind stress curl anomalies (WSCa), ENSO, $\mathrm{EKE}_{\mathrm{Sitka}}$, and $\mathrm{EKE}_{\mathrm{Haida}}$.

The time-dependent regression model with lags is expressed as

$$\hat{y}_t = \beta_0 + \sum_i \beta_i x_{i,t+\mathrm{lag}} + \varepsilon_t, \tag{3}$$

where $\hat{y}_t$ is the modeled pathway occurrence anomaly at time t, β_0 is the intercept (equal to the mean when all predictors are zero), β_i is the regression coefficient for predictor i, $x_{i,t+\mathrm{lag}}$ is the value of predictor i at time t + lag, and ε_t is the residual at time t. Lagged predictors were included to account for delayed oceanic responses.

f. Statistical tests

1) TIME SERIES CORRELATIONS

Statistical relationships between monthly time series of transport pathway relative occurrence were quantified using the Pearson correlation coefficients. Significance was assessed using the Student's t test, where the temporal autocorrelation was accounted for by estimating the effective degrees of freedom based on lag-1 autocorrelation, for each time series. The resulting effective degrees of freedom were used to compute the p values.

2) LINEAR REGRESSION MODEL ROBUSTNESS

Model robustness was assessed using a leave-one-predictor-out method. In this approach, each predictor was sequentially removed from the full regression model, and changes in explained variance r^2 were used to quantify its relative contribution. An F test was used to diagnose the statistical significance of each predictor.

3. Results

a. Evaluation of the reanalysis product

We first evaluate the reanalysis product's ability to capture the observed interannual variability in the Gulf of Alaska (0°–70°N and 170°–120°W, excluding the Bering Sea), over the period 1993–2025 (Figs. 1a–f). SST anomalies (SSTa) and SSHa are consistent with observations (Figs. 1a,b), specifically the warm anomalies during El Niño 1997/98 and the recent extremes such

Unauthenticated | Downloaded 11/19/26 07:19 PM UTC

as the Blob 2013/14, El Niño 2015, and the 2019 Alaska heat wave. It also captures the cold anomalies associated with the strong La Niña events in 1999, 2008, and 2012.

EKE is computed from surface velocity fields as deviations from the monthly mean flow and therefore represents mesoscale variability but does not include submonthly fluctuations. EKE from the ocean reanalysis product is generally consistent with observations throughout the time series (Figs. 1c,d). It successfully reproduces the seasonal cycle with a maximum in May, as well as the timing and magnitude of anomalous peaks, including the 1997/98 El Niño, and peaks in 2004, 2011, 2013, and 2016. The observed weakening in EKE during 2020–23 (Rallu De Malibran et al. 2024) is also well represented in GLORYSV12. This confirms that the reanalysis product adequately reproduces the variability in surface EKE, which is key to capture eddy-scale transport.

We compute the time derivative of normalized relative vorticity $|\partial(\zeta/f)/\partial t|$, a diagnostic of temporal variability in relative vorticity, following Rallu De Malibran et al. (2024). We compare the time-averaged spatial patterns between the reanalysis product and satellite-derived fields in Figs. 1e and 1f. This term can inform on where eddies are generated. The spatial structure is consistent between both fields, with elevated values along the Alaskan Coastal Current, specifically at the Haida and Sitka regions. Additionally, eddy generation sites are also captured along the Alaskan Stream, where the Yakutat eddies are formed (58°N, 145°W). These features are consistent with known locations of anticyclonic eddy formation along the Alaska Current. Although the present validation focuses primarily on surface quantities constrained by satellite observations, previous studies have shown that GLORYSV12 accurately reproduces upper-ocean temperature, salinity, and circulation variability, including subsurface dynamics and coastal variability (Amaya et al. 2023; Lellouche et al. 2013; Buongiorno Nardelli 2020; Verezemskaya et al. 2021). Buongiorno Nardelli (2020) showed that this reanalysis product generally exhibits small biases in near-surface velocities (at 15-m depth), including in the GOA.

Although the reanalysis exhibits minor biases, we show in Fig. S1 that it represents mesoscale eddies and their offshore propagation into the basin interior well. In addition, our sensitivity tests with particle release depths (Fig. S2) further indicate that the resulting transport pathways are robust across the upper ocean.

Particles were released in the Haida and Sitka regions (Fig. 1g) and advected within the reanalysis product current field. The Lagrangian trajectories reveal a consistent pattern as they follow the cyclonic circulation of the GOA through the Alaska Current and the Alaskan Stream, validating the reanalysis product's ability to represent the wide range of dynamics of the GOA (Stabeno et al. 2004; Combes et al. 2009; Ladd et al. 2009). Some trajectories interact with the eddy field and are carried offshore. Particles released near Haida Gwaii tend to recirculate at the coast, get trapped within Haida eddies, or get transported along the Alaska Current, where they may subsequently become trapped in eddies downstream. Some Haida trajectories display strong recirculation along the coast, where they either get retrained at the coast or leave the domain to the south and never join the cyclonic gyre circulation.

Particles released near Sitka display a more complex circulation pattern. Some trajectories are advected through the Alaskan Stream, with some flowing around Kodiak Island, while others get caught within mesoscale Sitka eddies and meander along the shelf break. Some trajectories are going against the general GOA cyclonic circulation and are transported southward and exported offshore within Haida eddies, making their way to the southeastern part of the basin.

b. Lagrangian transport pathways

1) SPATIOTEMPORAL EVOLUTION

We decompose the Haida Lagrangian trajectories into three dominant transport pathways based on their spatial and temporal evolution: 1) Gyre Circulation, 2) Offshore Export, and 3) Coastal Retention. These pathways reveal distinct physical regimes that govern how water released near Haida Gwaii disperses across the GOA (Fig. 2).

Particles in the Haida 1) Gyre Circulation pathway constitute 27% of the total trajectories. These particles are rapidly advected northward along the shelf break, into the subpolar gyre. First, they are entrained in the Alaska Current and eventually merge with the Alaskan Stream. These particles reach the northern GOA within 6 months, where some get caught within Sitka eddies and recirculate within the northeastern part of the basin. After 12 months, many particles in this pathway have reached the western boundary of the domain, with several recirculating within the gyre via the return flow, and the rest exiting the domain entirely. There are no particles from this pathway that remain near the original release site, indicative of efficient long-range export through this pathway.

The Haida 2) Offshore Export pathway captures 40% of the total trajectories and is the dominant pathway in this region. It represents waters that become entrained within the Haida mesoscale eddy field, including anticyclonic eddies, filaments, and surrounding mesoscale circulation features that transport coastal waters into the basin interior. These particles are retained and recirculate within the eddy field, with limited downstream gyre advection. After 12 months, they remain confined to the eastern part of the basin and most of them have not yet entered the gyre circulation. This pathway shows how mesoscale eddies contribute to cross-shelf exchange while retaining waters near the shelf break over an extended period of time.

The remaining Haida trajectories, which amount to 33% of the total trajectories, form the 3) Coastal Retention pathway. These trajectories remain in the coastal zone southeast of Haida Gwaii. The majority recirculate within the coastal boundary and remain confined, even after 12 months. Some exit the domain southward. These trajectories are likely influenced by weaker flow and limited offshore export.

After 12 months, the peak density regions (≥80% core density) of each pathway do not overlap, indicating that each of the Haida transport pathways follows a unique route that is driven by both local and large-scale circulation patterns.

Similar to the Haida trajectories, we examine the particle trajectories originating from the Sitka region and identify three distinct transport pathways (Fig. 3): 1) Gyre Circulation, 2) Offshore Export, and 3) Southward Coastal Retention.

Unauthenticated | Downloaded 11/19/26 07:19 PM UTC

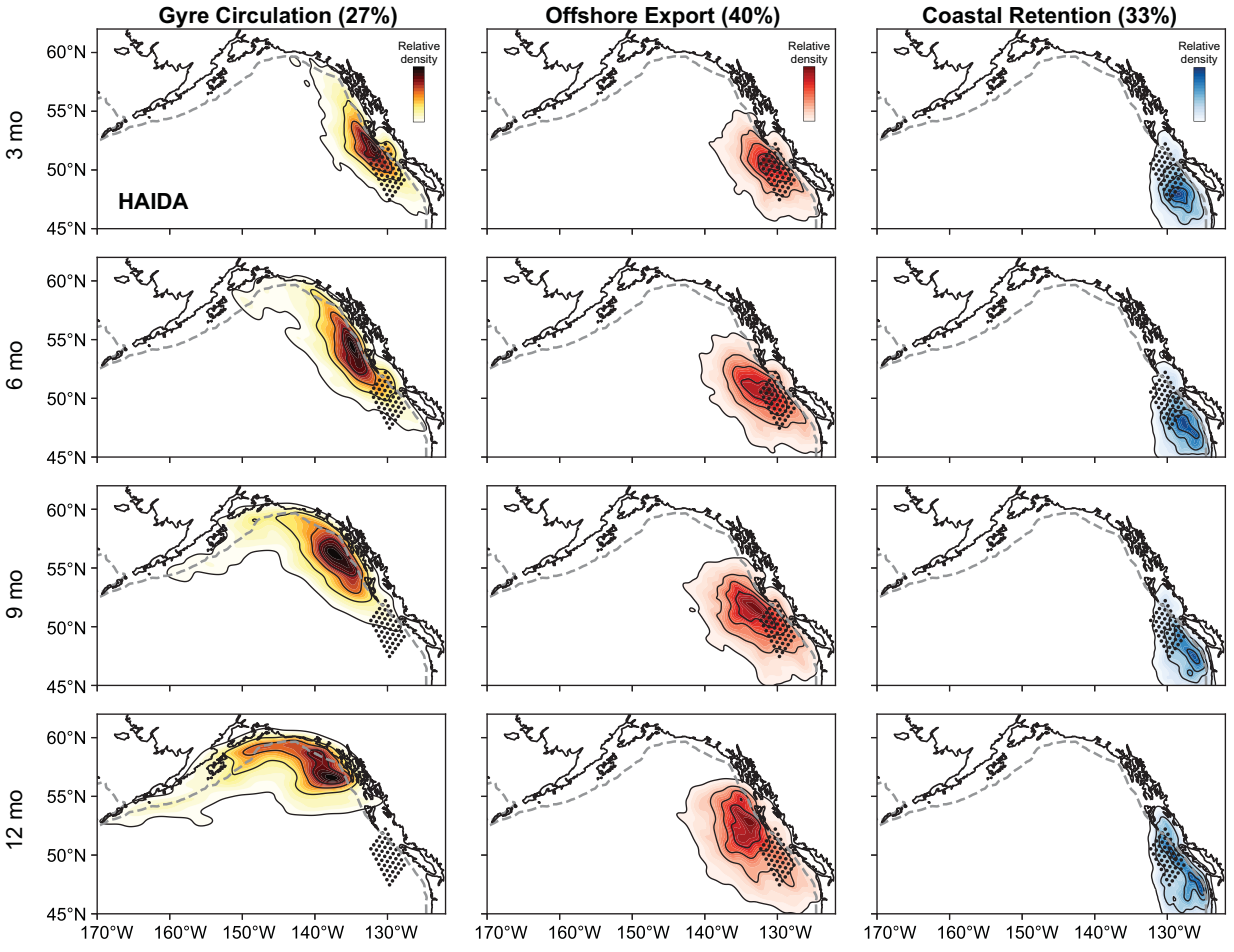


FIG. 2. Density maps of the Haida transport pathways and particle dispersion after 3, 6, 9, and 12 months: (left) Gyre Circulation (orange), (center) Offshore Export (red), and (right) Coastal Retention (blue). The gray dashed line shows the 500-m isobath, which marks the shelf break. Color intensity represents kernel density estimates (KDEs) of particle positions to visualize relative spatial concentration and highlight preferential dispersion pathways. Black isolines represent 20%, 40%, 60%, and 80% of the local peak density (KDE_{max}).

Particles that are in the Sitka 1) Gyre Circulation pathway constitute 16% of the total trajectories. They are similar to the Haida Gyre Circulation Pathway, entrained in the rapid gyre circulation. Since the particles are released much more north than the Haida trajectories, they immediately enter the Alaskan Stream and are advected westward along the shelf break and behind Kodiak Island and can sometimes be entrained within an eddy traveling along the Alaskan Stream. After 6 months, some trajectories spill over into the Bering Sea, and others leave the basin to the west. The rest recirculate within the subpolar gyre through the return flow, which is where most end up after 12 months. A small portion of particles, however, do remain behind potentially due to trapping in the Sitka eddy field.

The majority of the Sitka-released trajectories (81%) fall into the Sitka 2) Offshore Export pathway. This pathway represents the trajectories that are trapped within Sitka mesoscale eddies and recirculate within the shelf and shelfbreak region. After 3–6 months, most particles remain east of 145°W, but as time progresses, some get entrained in the Alaskan Stream. Gradually, most of them end up in the gyre-scale circulation and likely exit the basin or enter the return flow. While this transport pathway ends up on a similar trajectory to that of the Sitka Gyre Circulation Pathway, it is retained in the shelf area for the first few months, thanks to mesoscale eddies, contributing cross-shelf exchange of nutrient-rich coastal waters.

A small fraction of the trajectories (3%) follows a distinct 3) Southward Coastal Retention pathway into the Haida region. After 3–6 months, while most particles on this pathway are retained east of the basin, some particles reach the southernmost region of the basin and recirculate within the Haida Coastal Retention pathway region. Eventually, these particles join the gyre circulation. However, none of them reach the Alaskan Stream after 12 months, suggesting persistent retention, likely entrained by Haida and Sitka mesoscale eddies.

The relative concentration of these Sitka pathways demonstrates that while a portion of water is rapidly advected along the Alaskan Stream or travels southward, the majority is trapped

Unauthenticated | Downloaded 11/19/26 07:19 PM UTC

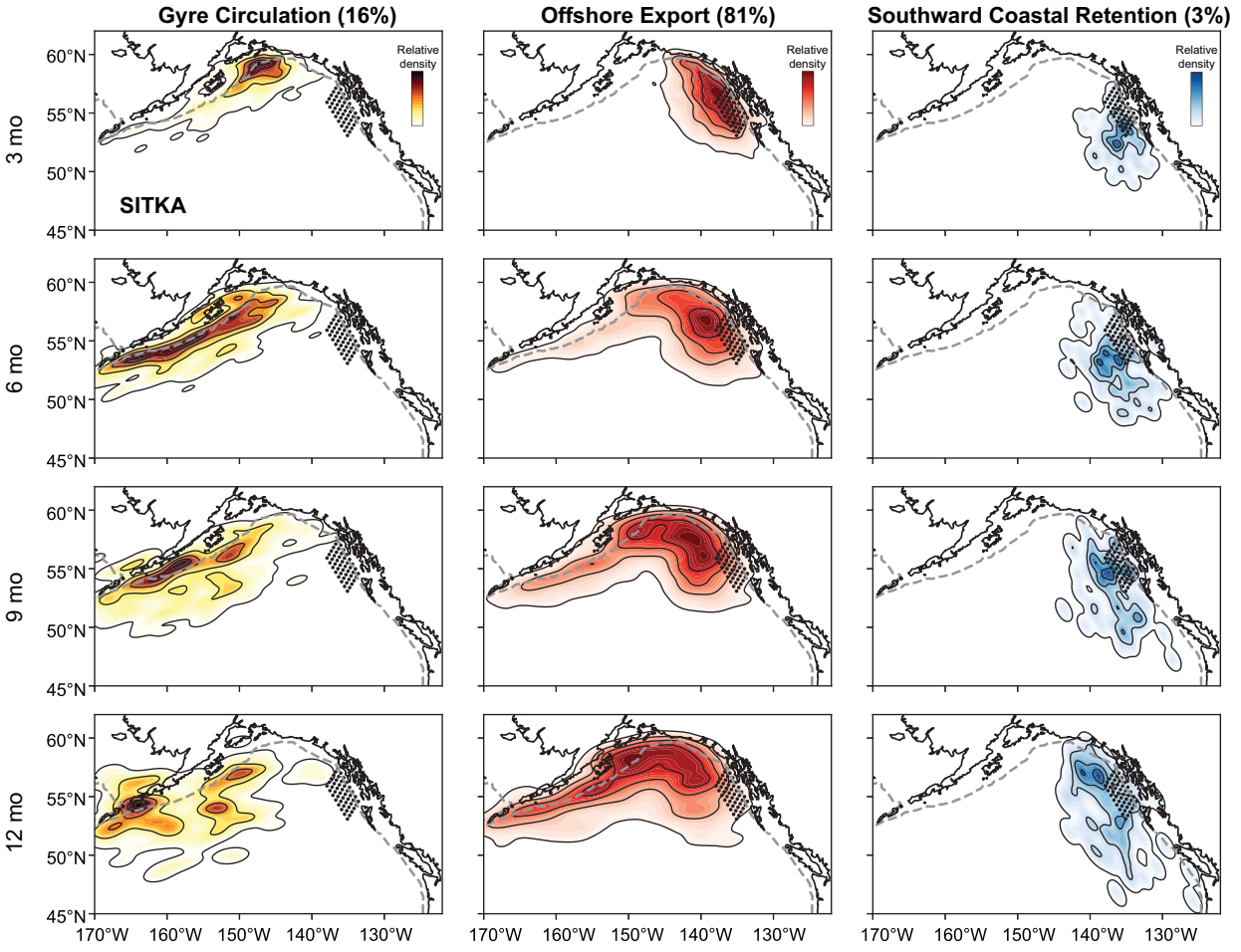


FIG. 3. As in Fig. 2, but for Sitka transport pathways: (left) Gyre Circulation (orange), (center) Offshore Export (red), and (right) Southward Coastal Retention (blue). The gray dashed line shows the 500-m isobath, which marks the shelf break. Color intensity represents the KDE of particle positions to visualize relative spatial concentration to highlight preferential dispersion pathways. Black isolines represent 20%, 40%, 60%, and 80% of the local peak density (KDE_{max}).

within Sitka eddies. This result highlights how eddies play an important role in recirculation and offshore export of the coastal waters.

2) SEASONAL AND INTERANNUAL VARIABILITY

All pathways display seasonal and interannual variability that is informative regarding connectivity of the GOA circulation dynamics and the impacts of atmospheric forcings on ocean transport.

For the Haida trajectories, we find that the Haida Gyre Circulation pathway and Haida Coastal Retention pathway display a strong seasonality (Fig. 4a). Between 25% and 31% of the particles follow the gyre circulation pathway, with a clear maximum in late fall and winter, which coincides with the peak downwelling-favorable wind conditions and strong gyre circulation. The minimum occurs during summer months, during the upwelling conditions and weakened gyre circulation. In contrast, the Haida Coastal Retention pathway shows an inverse relationship, with a peak occurrence of 35% in summer and a minimum of 27% in winter. These two pathways are significantly anticorrelated ($r = -0.63$, $p < 0.001$), suggesting that they are governed by the same wind-driven forcing but represent opposite outcomes in the coastal circulation response. The Haida Offshore Export pathway is the most dominant on average (~40%) and ranges from 37% in fall to 42% in winter.

The Haida Gyre Circulation pathway shows significant interannual variability. Just before the 1997/98 El Niño, almost 60% of the trajectories joined the Gyre Circulation, but that number declined sharply to 27% the following year. It was similarly suppressed after the 2015 and 2024 El Niño events, going from 30% to 25% and from 29% to 11%, respectively. These observations are consistent with the fact that El Niño is known to momentarily strengthen the Alaska Gyre through atmospheric teleconnections (Hristova et al. 2019). In recent years (2012–25), we find a significant suppression (t test, $p < 0.001$) in the Haida Gyre Circulation pathway, both in the mean and in the variance, which is consistent with persistent upwelling conditions and with previous observational studies (Rallu De Malibran et al. 2024).

Unauthenticated | Downloaded 11/19/26 07:19 PM UTC

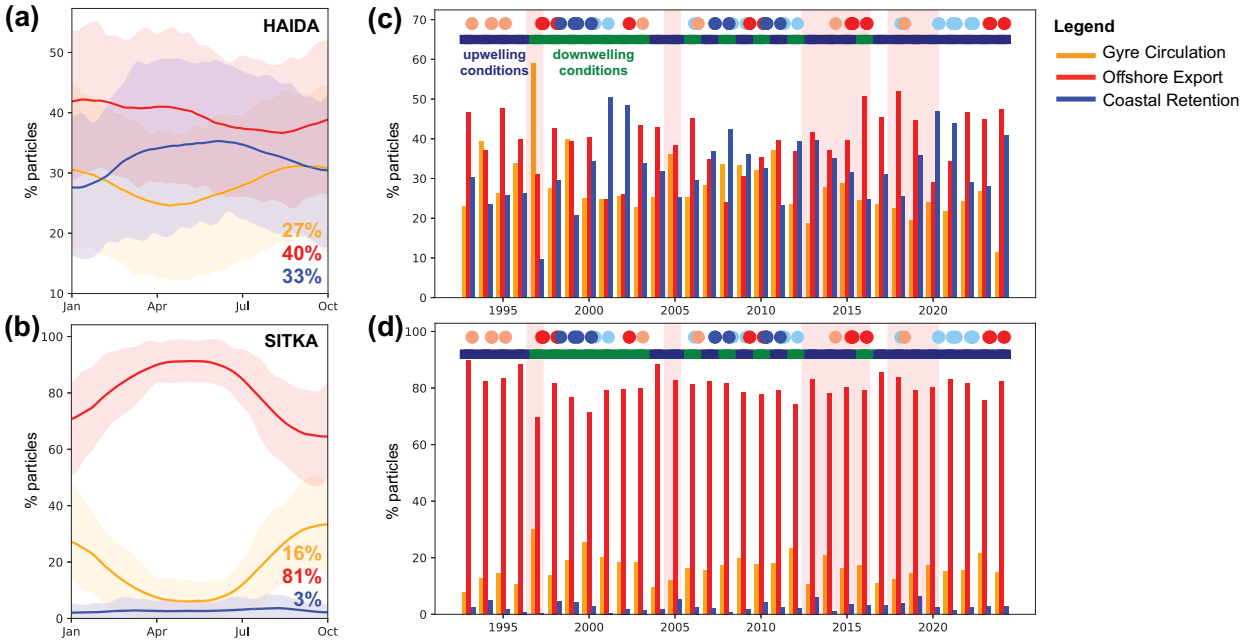


FIG. 4. Seasonal cycles for (a) Haida and (b) Sitka release sites, computed over the period 1993–2024. The lines correspond to the pathways in Figs. 2 and 3. The seasonal cycle is computed over daily averages, with the day of year recorded at the seeding date. The thick line shows the smoothed time series with a 60-day moving window. Note the difference in the y axis for the southbound pathway in (b). The shaded area shows the interannual spread in the seasonal cycle. (c),(d) The interannual time series are yearly averages of each pathway for Haida and Sitka. The scatter dots display years of strong and weak El Niño (red) and La Niña (blue) events, and the thick line shows years of upwelling (dark blue) and downwelling (green) conditions in the GOA. The MHWs are represented by the red shading.

While the Haida Offshore Export pathway is dominant in the climatological mean, its interannual variability is substantial. For instance, in contrast to the Haida Gyre Circulation pathway, Offshore Export was low before the 1997/98 El Niño and increased sharply the following year to 43%. Similarly, it increased substantially immediately following the 2015/16 El Niño, reaching an all-time high of 53%. It then dropped significantly to 31% in 2020 before increasing again during the weak but sustained La Niña conditions between 2020 and 2023, despite upwelling-favorable conditions, and remained elevated through the 2025 El Niño event (50%). The sudden increase after 2015 coincides with a period of increased EKE, which may reflect ENSO-related remote forcing acting on the coastal circulation. While downwelling equatorial Kelvin waves were present during the 2015/16 El Niño (Lin et al. 2025), their coastal extension in the GOA was weaker than during 1997/98 (Jacox et al. 2016; Capotondi et al. 2018). This suggests that the observed response likely reflects nonlinear interactions between remote ENSO forcing and regional atmospheric variability, rather than a direct Kelvin wave–driven signal.

The Haida Coastal Retention pathway exhibits a strong inverse relationship with the Haida Gyre Circulation pathway on interannual time scales, highlighting their shared sensitivity to wind-driven forcing. For instance, the Haida Coastal Retention pathway was suppressed prior to the 1997/98 El Niño event, followed by a sharp increase in 1998. It reached its peak (~50%) in 2002–03, coinciding with the end of a period of sustained downwelling-favorable conditions. This pathway was also more important during the 2013/14 Blob marine heat wave, and throughout that period, it consistently exceeded the weak Haida Gyre Circulation pathway. However, after the 2015/16 El Niño, the Haida Offshore Export pathway became dominant, and the coastal retention decreased simultaneously. The recent decade was also marked by a decreased gyre circulation pathway, likely driven by a combination of persistent upwelling-favorable winds, which slow down the gyre, and strong EKE variability.

Most of the Sitka trajectories (81%) get entrained in the Sitka Offshore Export pathway (Fig. 4b), which is by far the dominant pathway. It has strong seasonality and varies from 66% in winter to 91% in summer. About 16% of the Sitka trajectories are part of the Sitka Gyre Circulation pathway, where they are immediately advected in the Alaskan Stream. This pathway also displays a strong seasonality, peaking at 23% in winter and dropping to a minimum of 4% in summer. We find that the Sitka Gyre Circulation pathway and Offshore Export pathway are strongly anticorrelated ($r = -0.77$, $p \ll 0.001$). This dynamic is primarily driven by Sitka EKE. Specifically, the Sitka Offshore Export pathway is positively correlated with Sitka EKE ($r = -0.4$, $p < 0.05$), while the Sitka Gyre Circulation pathway is negatively correlated ($r = -0.4$, $p < 0.05$), both at a 3-month lag (Fig. S4). The remaining 3% of the trajectories move southward into the Haida eddy field. This pathway shows weak seasonality, with a maximum of 4% in early fall. The weak occurrence, seasonality, and large standard deviation of the southward transport pathway suggest that this pathway exists only under very specific conditions.

Unauthenticated | Downloaded 11/19/26 07:19 PM UTC

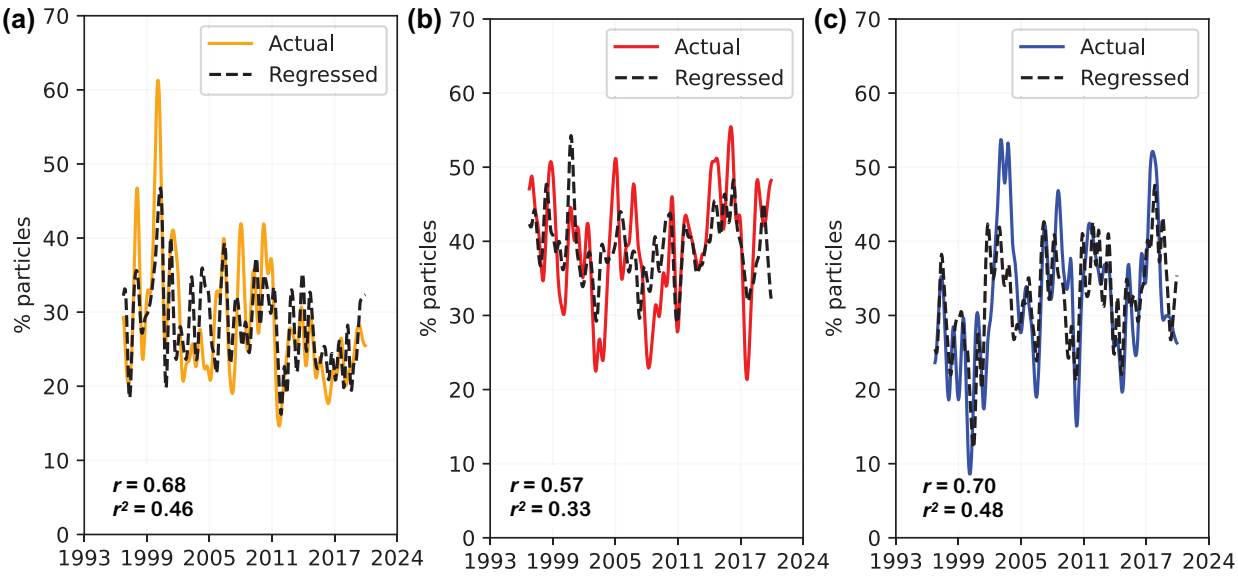


FIG. 5. Linear regression analysis for Haida (a) Gyre Circulation, (b) Offshore Export, and (c) Coastal Retention pathways. Solid lines show the occurrence percentages from the Lagrangian experiment, and dashed lines show the regression fit. Coefficients are listed in Table 2.

On an interannual time scale, the Sitka trajectories show similarities with those in the Haida region (Fig. 4d). For instance, the Sitka Gyre Circulation pathway peaks at 30% in 1997, just before the 1997/98 El Niño, and then weakens substantially to 17% the following year. A similar suppression is also observed during the 2015/16 El Niño. Throughout the entire study period, the Sitka Offshore Export pathway remains the dominant export mechanism for Sitka coastal waters. However, it experiences a strong reduction during the 1997/98 El Niño, a decrease that is compensated by a rise in the gyre circulation pathway. The Southward Coastal Retention pathway remains a minor and more episodic contributor (always <10%), nearly absent in 1997/98, and then increasing sharply the subsequent year, a pattern which is not clearly present after the 2010 and 2015/16 El Niño events. Although it shows no significant correlation with Sitka EKE, it does exhibit a weak but significant positive correlation ($r \sim 0.3$) with Haida EKE at a 2-month lag (Fig. S5). This suggests that the Sitka Southward Coastal Retention pathway may be modulated by eddy activity originating from the Haida region, potentially creating a meandering pathway through Haida eddies before reaching the southern GOA.

Unlike the Haida pathways, the Sitka Gyre Circulation and Offshore Export pathways do not show strong relationships with ENSO phases or upwelling/downwelling conditions. Interestingly, the Haida and Sitka Gyre Circulation pathways are significantly correlated with each other at lag 0 ($r = 0.4$, $p < 0.01$). Both Offshore Export pathways are also significantly correlated ($r = 0.4$, $p < 0.01$) with the Haida Offshore Export pathway lagging by approximately 3 months. This lag suggests that Haida trajectories respond to EKE variability later than Sitka trajectories, likely due to differences in their position relative to the eddy formation sites: Haida particles are released slightly upstream of the Haida eddy formation region, whereas Sitka particles are released within the Sitka eddy formation region. This spatial difference likely contributes to contrasting dynamical sensitivities between the two regions, with Sitka being more directly coupled to the Alaskan Stream and downstream export pathways and Haida more sensitive to basin-scale variability in gyre circulation and eddy generation.

c. *Quantifying contributions to transport*

To identify the drivers of different transport pathways of coastal water, we first computed lead–lag correlations between pathway occurrences and anomalies of SLP, SSH, wind stress, and wind stress curl (WSC) (Figs. S6–S11). Regions showing significant correlations ($p < 0.01$) were then used as predictors in linear regression models to quantify the pathways' response. The results are presented in Fig. 5 and Table 2 for Haida transport pathways and in Fig. 6 and Table 3 for Sitka transport pathways.

The Haida Gyre Circulation pathway responds to SLPa forcing associated with a deeper AL, as expected (Figs S6–S8, Fig. 5, Table 2). A stronger AL enhances Ekman transport and steepens the cross-shore SSH gradient, which intensifies the gyre circulation and favors this pathway. The Coastal Retention pathway significantly correlates with positive SLPa over the basin and is favored during a weaker gyre circulation. WSC is an important predictor of transport pathways. Positive anomalies are associated with surface divergence and enhanced Gyre Circulation and Offshore Export pathways, while negative anomalies are associated with surface convergence and increased Coastal Retention pathway. While SSH has a strong correlation with the transport pathways, we treat it as a lag response to SLPa and do not include it in the regression model. ENSO (with a 6-month lag) also has a significant correlation with the gyre and eddy pathways. We identify key aspects of the dynamics that help explain the observed distribution of transport pathways:

1) Positive WSC near the coast is associated with Ekman pumping and offshore Ekman transport, consistent with

Unauthenticated | Downloaded 11/19/26 07:19 PM UTC

TABLE 2. Statistics for Haida transport pathways. Coefficients for each transport type are listed, corresponding to the linear regressions shown in Fig. 5. Regression parameters include the variance explained r^2, the correlation, and corresponding coefficient β for each predictor. Bold coefficients highlight the significant values ($p < 0.01$), computed with the F test, which compares the explained variance when removing that predictor.

Coefficient	1) Gyre Circulation	2) Offshore Export	3) Coastal Retention
r^2	0.46	0.33	0.49
r	0.68	0.57	0.70
β_0	28.50	38.47	33.03
SLPa	**−2.82**	−1.10	**3.93**
τ_{y_ano}	−0.58	**−4.86**	**5.44**
WSCa	**4.14**	1.07	**−5.21**
ENSO (−6 months)	**1.88**	−0.93	−0.95
EKE_{Sitka_ano} (−6 months)	−0.48	−0.28	0.77
EKE_{Haida_ano}	**−1.30**	**1.95**	−0.65

reduced coastal retention and increased occurrence of Gyre Circulation and Offshore Export pathways. Conversely, negative WSC is associated with enhanced coastal convergence and increased coastal trapping.

2) Strong SLPa (deep AL) is associated with enhanced gyre transport of coastal waters via the Alaska Current, whereas a weak AL is associated with increased coastal trapping.
3) A deep AL is also associated with higher EKE, consistent with increased occurrence of the eddy transport pathway.
4) El Niño events are associated with increased gyre transport of coastal water, consistent with a deepened AL and intensified gyre circulation.
5) La Niña events are associated with enhanced eddy transport, potentially reflecting a redistribution of trajectories away from the Gyre Circulation pathway.
6) Enhanced Haida EKE is associated with increased eddy transport and reduced gyre transport of coastal water.

Although SLPa and meridional wind stress anomalies are closely related, sometimes wind stress emerges as a stronger predictor over SLPa, likely because it directly forces ocean circulation and better captures the mechanisms driving the pathway signal. The Haida Offshore Export pathway is the least well explained by the regression models, suggesting it is governed by nonlinear processes such as mesoscale variability or delayed oceanic responses (e.g., post–El Niño Kelvin waves). These may explain the transport peaks that occur after El Niño but are not captured by the atmospheric predictors alone.

The Sitka transport pathways exhibit strong relationships with atmospheric forcing (Figs. S9–S11, Fig. 6, Table 3). The Sitka Gyre Circulation pathway is strongly correlated with GOA SLPa, indicating that a deeper AL is associated with increased offshore transport into the Alaska Current. This response is consistent with the development of downwelling-favorable conditions and the associated northward alongshore wind stress. The Sitka Offshore Export pathway shows the opposite pattern: It is positively correlated with SLPa, indicating strong retention during weaker AL (upwelling conditions). WSC is also associated with the Sitka Offshore Export pathway,

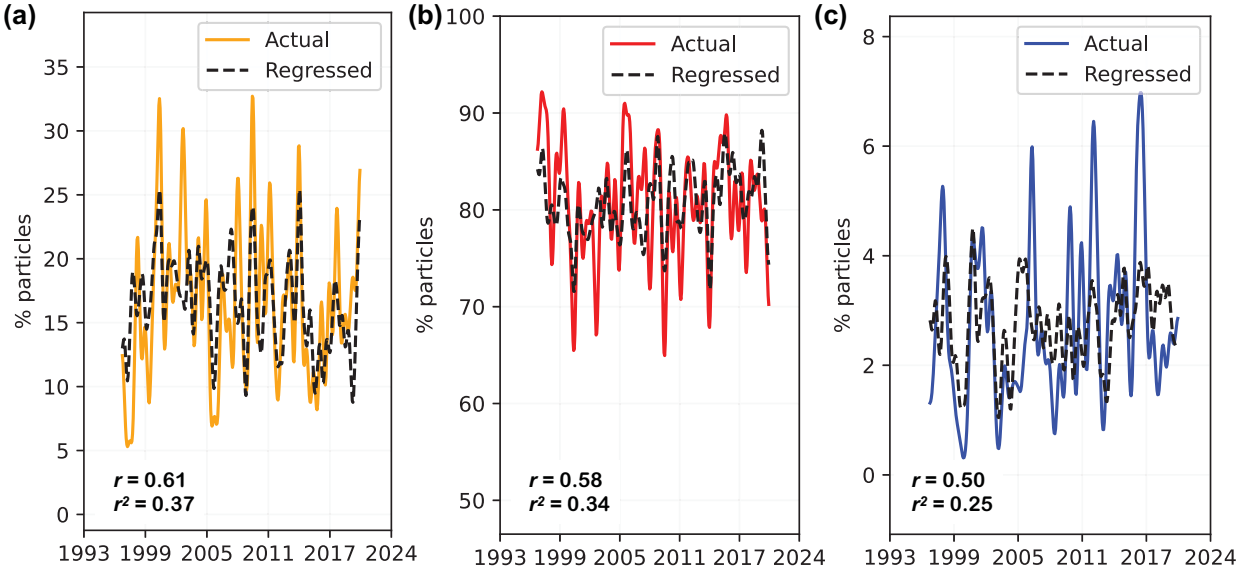


FIG. 6. As in Fig. 5, but for Sitka transport pathways.

Unauthenticated | Downloaded 11/19/26 07:19 PM UTC

TABLE 3. As in Table 2, but for Sitka, corresponding to the linear regression shown in Fig. 6.

Coefficient	1) Gyre Circulation	2) Offshore Export	3) Southward Coastal Retention
r^2	0.38	0.35	0.23
r	0.61	0.59	0.48
β_0	17.09	80.25	2.66
SLPa	−0.14	0.16	−0.03
τ_{y_ano}	**2.20**	**−2.41**	0.21
WSCa	1.29	−0.50	**−0.79**
ENSO (−6 months)	0.20	0.28	**−0.48**
EKE_{Sitka_ano}	**−1.24**	**1.56**	**−0.32**
EKE_{Haida_ano} (−3 months)	**1.15**	**−1.74**	**0.59**

suggesting a role in modulating coastal retention and offshore transport. The Sitka Coastal Retention Southward pathway is more spatially confined to the southeastern GOA and correlates with southern Ekman downwelling. This pathway is more difficult to interpret, though Haida EKE (3-month lag) shows evidence of being an important factor. Examining each predictive factor for the Sitka pathways, we observe the following characteristics of the atmospheric dynamics that could help explain the pathway distributions:

1) WSC and Ekman pumping are associated with increased coastal retention.
2) Strong SLPa (deep AL) and associated northward alongshore wind stress are linked to increased export into the gyre circulation via the Alaskan Stream.
3) Weak SLPa is associated with enhanced eddy transport.
4) High Sitka EKE is associated with increased eddy-driven transport and reduced gyre circulation trajectories.
5) ENSO is not a dominant predictor of these transport pathways.
6) The Southward Coastal Retention pathway relies on Ekman pumping and elevated Haida EKE, which together are associated with southward meandering of coastal water.

Note that points 2 and 3 are consistent with the behavior of the Haida transport pathways, indicating that gyre circulation and offshore export pathways covary with similar atmospheric drivers.

4. Summary and discussion

In this study, we used Lagrangian trajectories to identify dominant transport pathways of coastal water in the Gulf of Alaska. We assessed the relationship between each pathway and the large-scale and localized atmospheric and oceanic forcings. This approach allows us to distinguish between along-shelf and cross-shelf transport mechanisms, which are difficult to separate with a Eulerian framework.

We released particles in two key coastal regions, Haida Gwaii and Sitka, and identified three dominant transport regimes corresponding to gyre circulation, mesoscale eddy transport export, and coastal retention. These dynamics are consistent with established circulation patterns in the GOA. Specifically, the Gyre Circulation pathway aligns with the fast-flowing Alaskan Stream (Reed 1984), while the offshore export pathway overlaps with regions of enhanced offshore mesoscale variability (Ladd 2007; Ladd et al. 2009) and associated high chlorophyll anomalies (Combes et al. 2013; Rallu De Malibran et al. 2024). The Coastal Retention pathway reflects more localized transport and limited offshore export near the shelf break.

Our results demonstrate that large-scale atmospheric forcing plays a key role in modulating coastal water trajectories in the GOA, suggesting a potential source of predictability in their transport. Variability in transport pathways reflects the lagged response of mesoscale dynamics to atmospheric forcing, such that sustained atmospheric anomalies are associated with changes in particle trajectories. Specifically, SLPa, local wind stress, WSCa, ENSO, and regional EKE collectively explain between 23% and 49% of the variance in pathway occurrences, indicating potential predictive lead time for pathway dominance on seasonal-to-interannual time scales. ENSO and the integrated ocean response to large-scale SLPa exhibit predictive skill for intrabasin atmospheric dynamics (Di Lorenzo and Mantua 2016), and our results suggest that these same modes of variability are also relevant for mesoscale transport and coastal exchange of nutrient-rich waters. Moreover, local WSC near the particle release sites emerges as an important predictor of cross-shelf exchange: Ekman pumping is associated with enhanced offshore transport and increased likelihood of particles entering gyre or eddy pathways, whereas Ekman suction is linked to increased coastal retention.

Figure 7 provides a conceptual synthesis of the transport regimes identified in this study. Under normal (downwelling) conditions (Fig. 7a), associated with a deepened AL, coastal waters are preferentially exported alongshore within the gyre circulation, and the seasonal formation of mesoscale eddies facilitates cross-shelf exchange between the coastal margin and the interior GOA. In contrast, under sustained upwelling-favorable conditions associated with weakened SLPa (weakened AL) during marine heat waves (Fig. 7b), such as the 2013–16 period, weakened gyre circulation reduces alongshore transport and generally suppresses eddy formation, thereby increasing coastal retention. However, episodic El Niño events occurring within this period can temporarily boost mesoscale activity and thereby eddy-driven export, sustaining cross-shelf exchange of nutrient-rich coastal waters. While this schematic provides a general overview of the transport pathway dynamics, regional differences in coastal water trajectories exist, particularly between the Haida Gwaii and Sitka regions.

The Sitka pathways are associated with simpler dynamics due to the release site's proximity to the Alaskan Stream and

Unauthenticated | Downloaded 11/19/26 07:19 PM UTC

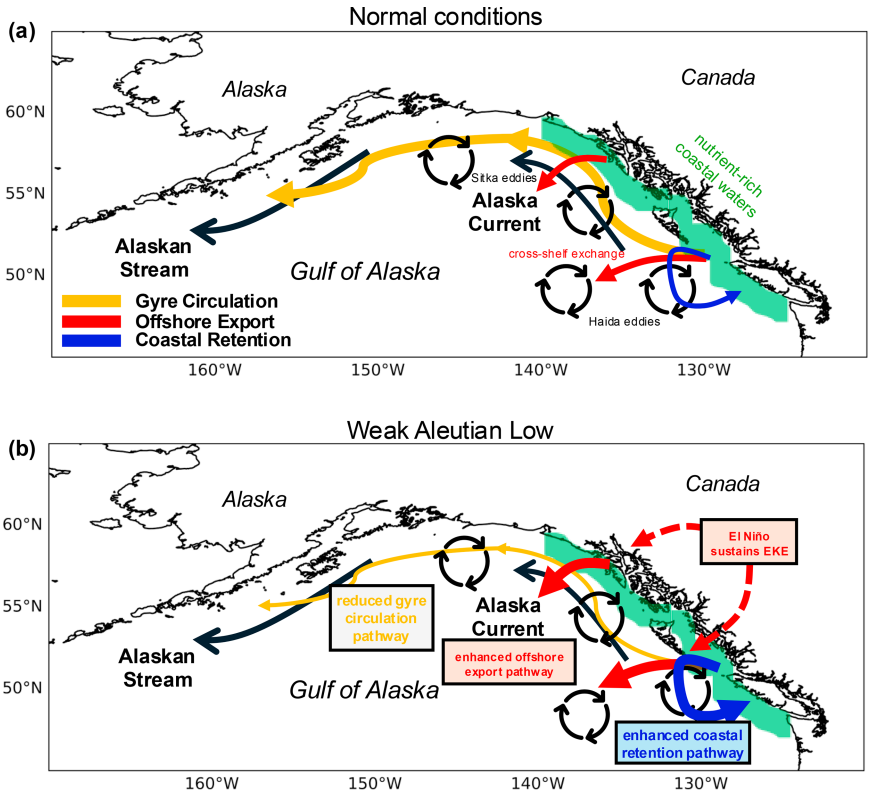


FIG. 7. Schematic for transport pathways of GOA coastal waters under (a) normal conditions and (b) weak AL conditions associated with the MHWs between 2013 and 2019.

the Sitka eddy field. Sitka particles were predominantly entrained into the Sitka eddy field or advected downstream in the Alaskan Stream. While the regressions explained less variance than for the Haida pathways, the fate of those trajectories was more easily explained and more directly tied to a dominant flow feature, namely, the local wind stress, which results from SLPa. A stronger wind stress increased gyre transport, while a weaker wind stress increased the Sitka Offshore Export pathway. The southward pathway, although infrequent (~3%), represented an exception as it opposed the mean circulation. It occurred during periods of negative WSCa and elevated Haida EKE, during which particle trajectories were advected southward and reached the southern portion of the basin.

A notable similarity exists between the Haida Gyre Circulation pathway and the Sitka Offshore Export pathway, as trajectories in both cases ultimately follow the Alaskan Stream within 12 months after release. This resemblance reflects connectivity in the regional ocean dynamics and methodological choices in pathway definition. Haida eddies, guided by the Alaska Current, propagate toward regions where Sitka eddies form, and both Haida- and Sitka-origin eddies eventually end up in the Alaskan Stream. Particles released in the Haida region may be entrained into Sitka eddies and vice versa with Sitka-released particles entrained into Haida eddies. Travel time also contributes to the observed overlap: The Sitka region is much closer to the Alaskan Stream, so offshore advection occurs more rapidly (starting after 3 months), whereas Haida particles following the gyre circulation pathway require 6–9 months to reach the Sitka region.

In general, our findings suggest the following:

1) Ekman pumping (or WSC) is the dominant predictor of whether transport remains coastal or becomes offshore.
2) Gyre circulation, associated with SLPa and local wind stress, influences whether coastal waters advected offshore enter the gyre (alongshore transport) or are exported by mesoscale eddies (cross-shore transport).
3) Coastal waters advected offshore can be trapped and transported by mesoscale eddies generated in the Haida or Sitka regions, contributing to cross-shelf exchange.
4) El Niño events are primarily associated with variability of coastal water transport along the gyre circulation, indirectly linked to changes in SLPa, wind stress, and mesoscale EKE, with the response differing between events.

These results suggest that knowledge of the northeast Pacific atmospheric state can help anticipate the dominant transport pathways and coastal–offshore exchange in the GOA.

a. Limitations

One of the challenges with this mechanistic interpretation is that SLPa, coastal wind stress, and EKE are not fully independent. For example, EKE reflects the integrated response of mesoscale dynamics across overlapping time scales, including both

Unauthenticated | Downloaded 11/19/26 07:19 PM UTC

direct atmospheric forcing and the evolution and recirculation of preexisting eddies within the background flow. While EKE often increases following strong winter winds through enhanced downwelling-favorable conditions and Ekman transport, it can also persist due to nonlinear eddy–eddy interactions and the background circulation.

Although the regressions capture key relationships between transport pathways and atmospheric and oceanic variables, they explain only part of the total variability. This likely reflects the nonlinear and more complex response of mesoscale variability to external forcings such as Kelvin waves (Melsom et al. 1999), mean-flow interactions (Kang and Curchitser 2015), and changes in baroclinicity (Shore et al. 2008), which are not explicitly captured in the linear regression framework. These processes, along with ocean memory and cumulative effects of forcing, are difficult to resolve and limit the predictability of EKE.

It is important to note that the regression framework presented here quantifies (lagged) covariance between atmospheric and oceanic forcing and transport pathway variability, rather than providing a predictive model of coastal water trajectories. The oceanic response is interpreted as an integrated adjustment to atmospheric forcing over time scales of months, which are comparable to the transit times of Lagrangian trajectories from coast to basin interior.

Despite these limitations, the regression model nonetheless confirms strong connections between mesoscale EKE and eddy transport pathways. Yet, there are key differences between Eulerian EKE and Lagrangian eddy transport pathways. The Haida Offshore Export pathway, despite its close ties to Haida EKE, did not exhibit a seasonal cycle. This indicates its variability is driven over interannual, not seasonal, time scales.

b. *Connection to broader context*

This analysis establishes a mechanistic understanding of the ways that climate-driven forcing affects ecosystem dynamics in the GOA, particularly in the context of the recent years of marine heat waves (2013–20). While Rallu De Malibran et al. (2024) found that the generation of anticyclonic eddies was suppressed during the recent MHWs, this did not necessarily lead to a reduction in the overall cross-shelf transport. This distinction is critical, as we find in this study that the persistence of the eddy field is sufficient to maintain cross-shelf transport pathways. We did not find a direct relationship between MHWs and the Offshore Export pathways, only a reduction in the gyre circulation pathways associated with a weakening of the AL. This stability in offshore export was partly due to the 2015/16 El Niño, which momentarily strengthened the AL and brought a resurgence of Haida and Sitka EKE. These findings suggest that mesoscale eddies can still promote cross-shelf exchange despite broader climate conditions that might suppress their formation. This supports the findings from Litzow et al. (2020), which found no evidence for large-scale ecosystem reorganization during 2014–19 in the GOA. Thus, despite periods of persistent weakening of the subpolar gyre circulation linked to the recent marine heat waves (e.g., the Blob, 2013/14, the 2019 Alaska heat wave), our results demonstrate that episodic El Niño events, along with ocean memory provided by slow-moving long-lived mesoscale eddies, are crucial for maintaining the cross-shelf exchange of nutrient-rich coastal waters into the nutrient-limited basin interior. These processes help sustain offshore nutrient supply and therefore represent key mechanisms supporting marine ecosystem resilience under extreme climate conditions.

5. Conclusions

This study used Lagrangian particle tracking to link coastal water transport in the GOA to large-scale atmospheric drivers and mesoscale eddy dynamics over the period 1993–2025. Variability in each transport pathway was associated with distinct atmospheric drivers and modes of the northeast Pacific, suggesting a strong potential for seasonal-to-interannual predictability of cross-shelf exchange of nutrient-rich waters in the region.

The framework presented in this study provides a valuable tool for evaluating how climate-driven shifts in circulation may alter marine ecosystems. Future studies should explore how nonlinear dynamics and long-term changes in ocean properties also impact coastal water transport. This would enhance the ability of the scientific community and resource managers to anticipate ecological shifts, which is crucial for fisheries management and regional climate adaptation in the northeast Pacific.

Acknowledgments. This work was supported by the National Science Foundation under NSF Grant OCE-1948627. AJM was partly supported by NSF Grant OCE-2224726. MAF was partly supported by NASA Grants 80NSSC24M0143 and 80NSSC24K1422. The authors thank Baylor Fox-Kemper, Jack Mustard, and Yusen Liu for their insightful discussions and constructive feedback, which greatly improved the analysis and interpretation of the results.

Data availability statement. All datasets used in this study are publicly available and described in section 2. Further information on the model setups and analysis tools can be obtained directly from the corresponding author.

REFERENCES

Almeida, L. Z., B. J. Laurel, H. L. Thalmann, and J. A. Miller, 2024: Warmer, earlier, faster: Cumulative effects of Gulf of Alaska heatwaves on the early life history of Pacific cod. *Elementa*, **12**, 00050, https://doi.org/10.1525/elementa.2023.00050.

Amaya, D. J., A. J. Miller, S.-P. Xie, and Y. Kosaka, 2020: Physical drivers of the summer 2019 North Pacific marine heatwave. *Nat. Commun.*, **11**, 1903, https://doi.org/10.1038/s41467-020-15820-w.

——, M. G. Jacox, M. A. Alexander, J. D. Scott, C. Deser, A. Capotondi, and A. S. Phillips, 2023: Bottom marine heatwaves along the continental shelves of North America. *Nat. Commun.*, **14**, 1038, https://doi.org/10.1038/s41467-023-36567-0.

Batten, S. D., C. Ostle, P. Hélaouët, and A. W. Walne, 2022: Responses of Gulf of Alaska plankton communities to a marine heat wave. *Deep-Sea Res. II*, **195**, 105002, https://doi.org/10.1016/j.dsr2.2021.105002.

Unauthenticated | Downloaded 11/19/26 07:19 PM UTC

Bond, N. A., M. F. Cronin, H. Freeland, and N. Mantua, 2015: Causes and impacts of the 2014 warm anomaly in the NE Pacific. *Geophys. Res. Lett.*, **42**, 3414–3420, https://doi.org/10.1002/2015GL063306.

Boyd P. W., F. A. Whitney, P. J. Harrison, and C. S. Wong, 1995: The NE subarctic Pacific in winter: II. Biological rate processes. *Mar. Ecol. Prog. Ser.*, **128**, 25–34, https://doi.org/10.3354/meps128025.

Buongiorno Nardelli, B., 2020: A multi-year time series of observation-based 3D horizontal and vertical quasi-geostrophic global ocean currents. *Earth Syst. Sci. Data*, **12**, 1711–1723, https://doi.org/10.5194/essd-12-1711-2020.

Capotondi, A., P. D. Sardeshmukh, and L. Ricciardulli, 2018: The nature of the stochastic wind forcing of ENSO. *J. Climate*, **31**, 8081–8099, https://doi.org/10.1175/JCLI-D-17-0842.1.

Combes, V., and E. Di Lorenzo, 2007: Intrinsic and forced interannual variability of the Gulf of Alaska mesoscale circulation. *Prog. Oceanogr.*, **75**, 266–286, https://doi.org/10.1016/j.pocean.2007.08.011.

——, ——, and E. Curchitser, 2009: Interannual and decadal variations in cross-shelf transport in the Gulf of Alaska. *J. Phys. Oceanogr.*, **39**, 1050–1059, https://doi.org/10.1175/2008JPO4014.1.

——, F. Chenillat, E. Di Lorenzo, P. Rivière, M. Ohman, and S. Bograd, 2013: Cross-shore transport variability in the California Current: Ekman upwelling vs. eddy dynamics. *Prog. Oceanogr.*, **109**, 78–89, https://doi.org/10.1016/j.pocean.2012.10.001.

Crawford, W. R., 2005: Heat and fresh water transport by eddies into the Gulf of Alaska. *Deep-Sea Res. II*, **52**, 893–908, https://doi.org/10.1016/j.dsr2.2005.02.003.

——, J. Y. Cherniawsky, M. G. G. Foreman, and J. F. R. Gower, 2002: Formation of the Haida-1998 oceanic eddy. *J. Geophys. Res.*, **107**, 6-1–6-11, https://doi.org/10.1029/2001JC000876.

Cullen, J. T., M. Chong, and D. Ianson, 2009: British Columbian continental shelf as a source of dissolved iron to the subarctic northeast Pacific Ocean. *Global Biogeochem. Cycles*, **23**, GB4012, https://doi.org/10.1029/2008GB003326.

Di Lorenzo, E., and N. Mantua, 2016: Multi-year persistence of the 2014/15 North Pacific marine heatwave. *Nat. Climate Change*, **6**, 1042–1047, https://doi.org/10.1038/nclimate3082.

Hauri, C., R. Pagès, K. Hedstrom, S. C. Doney, S. Dupont, B. Ferriss, and M. F. Stuecker, 2024: More than marine heatwaves: A new regime of heat, acidity, and low oxygen compound extreme events in the Gulf of Alaska. *AGU Adv.*, **5**, e2023AV001039, https://doi.org/10.1029/2023AV001039.

Hayes, P., S. Augustine, M. Hatch, and L. McClenachan, 2025: Ecological legacy of indigenous dispossession: Disruption of ancestral sea gardens by commercial clam fisheries in British Columbia, 1882–1985. *Philos. Trans. Roy. Soc.*, **B380**, 20240277, https://doi.org/10.1098/rstb.2024.0277.

Hristova, H. G., C. Ladd, and P. J. Stabeno, 2019: Variability and trends of the Alaska Gyre from Argo and satellite altimetry. *J. Geophys. Res. Oceans*, **124**, 5870–5887, https://doi.org/10.1029/2019JC015231.

Ito, T., A. H. V. Timmerman, A. Bjouklund, S. I. Stanley, Y. Abe, C. T. Reinhard, and J. Montoya, 2026: Eddy-induced iron transport sustains the biological productivity in the Gulf of Alaska. *J. Geophys. Res. Oceans*, **131**, e2025JC022996, https://doi.org/10.1029/2025JC022996.

Jacox, M. G., E. L. Hazen, K. D. Zaba, D. L. Rudnick, C. A. Edwards, A. M. Moore, and S. J. Bograd, 2016: Impacts of the 2015–2016 El Niño on the California Current System: Early assessment and comparison to past events. *Geophys. Res. Lett.*, **43**, 7072–7080, https://doi.org/10.1002/2016GL069716.

Jean-Michel, L., and Coauthors, 2021: The Copernicus global 1/12° oceanic and sea ice GLORYS12 reanalysis. *Front. Earth Sci.*, **9**, 698876, https://doi.org/10.3389/feart.2021.698876.

Kang, D., and E. N. Curchitser, 2015: Energetics of eddy–mean flow interactions in the Gulf Stream region. *J. Phys. Oceanogr.*, **45**, 1103–1120, https://doi.org/10.1175/JPO-D-14-0200.1.

Ladd, C., 2007: Interannual variability of the Gulf of Alaska eddy field. *Geophys. Res. Lett.*, **34**, L11605, https://doi.org/10.1029/2007GL029478.

——, W. R. Crawford, C. E. Harpold, W. K. Johnson, N. B. Kachel, P. J. Stabeno, and F. Whitney, 2009: A synoptic survey of young mesoscale eddies in the eastern Gulf of Alaska. *Deep-Sea Res. II*, **56**, 2460–2473, https://doi.org/10.1016/j.dsr2.2009.02.007.

Lellouche, J.-M., and Coauthors, 2013: Evaluation of global monitoring and forecasting systems at Mercator Océan. *Ocean Sci.*, **9**, 57–81, https://doi.org/10.5194/os-9-57-2013.

Lin, Y.-F., and Coauthors, 2025: Diverse NPMM conditions deviate the 2023/24 El Niño from the 1997/1998 and 2015/2016 extreme El Niño events. *npj Climate Atmos. Sci.*, **8**, 133, https://doi.org/10.1038/s41612-025-01013-z.

Litzow, M. A., and Coauthors, 2020: Evaluating ecosystem change as Gulf of Alaska temperature exceeds the limits of preindustrial variability. *Prog. Oceanogr.*, **186**, 102393, https://doi.org/10.1016/j.pocean.2020.102393.

McKinstry, C. A., R. W. Campbell, and K. Holderied, 2022: Influence of the 2014–2016 marine heatwave on seasonal zooplankton community structure and abundance in the lower Cook Inlet, Alaska. *Deep-Sea Res. II*, **195**, 105012, https://doi.org/10.1016/j.dsr2.2021.105012.

Melsom, A., S. D. Meyers, J. J. O'Brien, H. E. Hurlburt, and J. E. Metzger, 1999: ENSO effects on Gulf of Alaska eddies. *Earth Interact.*, **3**, https://doi.org/10.1175/1087-3562(1999)003%3C0001:EEOGOA%3E2.3.CO;2.

Okkonen, S. R., T. J. Weingartner, S. L. Danielson, D. L. Musgrave, and G. M. Schmidt, 2003: Satellite and hydrographic observations of eddy-induced shelf-slope exchange in the northwestern Gulf of Alaska. *J. Geophys. Res.*, **108**, 3033, https://doi.org/10.1029/2002JC001342.

Rallu De Malibran, M. C., C. M. Kaplan, and E. Di Lorenzo, 2024: Marine heatwaves suppress ocean circulation and large vortices in the Gulf of Alaska. *Commun. Earth Environ.*, **5**, 622, https://doi.org/10.1038/s43247-024-01785-x.

Reed, R., 1984: Flow of the Alaskan Stream and its variations. *Deep-Sea Res.*, **31A**, 369–386, https://doi.org/10.1016/0198-0149(84)90090-6.

Rovegno, P. S., C. A. Edwards, and K. W. Bruland, 2009: Observations of a Kenai Eddy and a Sitka Eddy in the northern Gulf of Alaska. *J. Geophys. Res.*, **114**, C11012, https://doi.org/10.1029/2009JC005451.

Shore, J., M. W. Stacey, and D. G. Wright, 2008: Sources of eddy energy simulated by a model of the northeast Pacific Ocean. *J. Phys. Oceanogr.*, **38**, 2283–2293, https://doi.org/10.1175/2008JPO3800.1.

Stabeno, P., N. Bond, A. Hermann, N. Kachel, C. Mordy, and J. Overland, 2004: Meteorology and oceanography of the northern Gulf of Alaska. *Cont. Shelf Res.*, **24**, 859–897, https://doi.org/10.1016/j.csr.2004.02.007.

Suryan, R. M., and Coauthors, 2021: Ecosystem response persists after a prolonged marine heatwave. *Sci. Rep.*, **11**, 6235, https://doi.org/10.1038/s41598-021-83818-5.

Tabata, S., 1982: The anticyclonic, baroclinic eddy off Sitka, Alaska, in the northeast Pacific Ocean. *J. Phys. Oceanogr.*, **12**,

Unauthenticated | Downloaded 11/19/26 07:19 PM UTC

1260–1282, https://doi.org/10.1175/1520-0485(1982)012%3C1260:TABEOS%3E2.0.CO;2.

Ueno, H., K. Sato, H. J. Freeland, W. R. Crawford, H. Onishi, E. Oka, and T. Suga, 2009: Anticyclonic eddies in the Alaskan Stream. *J. Phys. Oceanogr.*, **39**, 934–951, https://doi.org/10.1175/2008JPO3948.1.

Verezemskaya, P., B. Barnier, S. K. Gulev, S. Gladyshev, J. Molines, V. Gladyshev, J. Lellouche, and A. Gavrikov, 2021: Assessing eddying (1/12°) ocean reanalysis GLORYS12 using the 14-yr instrumental record from 59.5°N section in the Atlantic. *J. Geophys. Res. Oceans*, **126**, e2020JC016317, https://doi.org/10.1029/2020JC016317.

Weitzman, B., and Coauthors, 2021: Changes in rocky intertidal community structure during a marine heatwave in the northern Gulf of Alaska. *Front. Mar. Sci.*, **8**, 556820, https://doi.org/10.3389/fmars.2021.556820.

Whitney, F., and M. Robert, 2002: Structure of Haida eddies and their transport of nutrient from coastal margins into the NE Pacific Ocean. *J. Oceanogr.*, **58**, 715–723, https://doi.org/10.1023/A:1022850508403.

Wyatt, A. M., L. Resplandy, and A. Marchetti, 2022: Ecosystem impacts of marine heat waves in the northeast Pacific. *Biogeosciences*, **19**, 5689–5705, https://doi.org/10.5194/bg-19-5689-2022.

Unauthenticated | Downloaded 11/19/26 07:19 PM UTC